Molecular Biology of the Cell
Vol. 19, 5156–5167, December 2008

The C-Terminal Tail Region of Nonmuscle Myosin II Directs Isoform-specific Distribution in Migrating Cells

Joshua C. Sandquist* and Anthony R. Means

Department of Pharmacology and Cancer Biology, Duke University Medical Center; Durham, NC 27710

Submitted May 29, 2008; Revised September 19, 2008; Accepted September 30, 2008
Monitoring Editor: Yu-Li Wang

Nonmuscle myosin II isoforms A and B (hereafter, IIA and IIB) perform unique roles in cell migration, even though both isoforms share the same basic molecular functions. That IIA and IIB assume distinct subcellular distribution in migrating cells suggests that discrete spatiotemporal regulation of each isoform's activity may provide a basis for its unique migratory functions. Here, we make the surprising finding that swapping a small C-terminal portion of the tail between IIA and IIB inverts the distinct distribution of these isoforms in migrating cells. Moreover, swapping this region between isoforms also inverts their specific turnover properties, as assessed by fluorescence recovery after photobleaching and Triton solubility. These data, acquired through the use of chimeras of IIA and IIB, suggest that the C-terminal region of the myosin heavy chain supersedes the distinct motor properties of the two isoforms as the predominant factor directing isoform-specific distribution. Furthermore, our results reveal a correlation between isoform solubility and distribution, leading to the proposal that the C-terminal region regulates isoform distribution by tightly controlling the amount of each isoform that is soluble and therefore available for redistribution into new protrusions.

INTRODUCTION

Nonmuscle myosin II (hereafter myosin II) is an essential component of the cell's migration machinery, and recent evidence suggests that the different myosin II isoforms make unique contributions to the motile process (Sandquist *et al*., 2006; Even-Ram *et al*., 2007; Vicente-Manzanares *et al*., 2007). Cell migration has been described as a cycle of coordinated steps including polarized protrusion of membrane, formation and turnover of adhesive complexes, cell body translocation, and tail deadhesion and retraction. Myosin II-based contractility has been observed to function, directly or indirectly, in each of these steps, demonstrating the importance of this motor protein for proper motility (Chrzanowska-Wodnicka and Burridge, 1996; Lauffenburger and Horwitz, 1996; Worthylake and Burridge, 2003; Conti and Adelstein, 2008). Considering the importance of cell migration to a broad range of both physiological and pathological processes, it is not surprising that much current research is focused upon understanding the many ways by which myosin II contributes to cell motility.

A molecule of myosin II consists of six peptides, arranged as a dimer of heavy chains with one essential light chain (ELC) and one regulatory light chain (RLC) tightly but noncovalently associated with each heavy chain (Warrick and Spudich, 1987; see Figure 4A). Three separate genes for the nonmuscle myosin heavy chains (NMHC) have been identified in mammals, giving rise to three isoforms of the myosin II protein complex, referred to here as IIA, IIB, and IIC (Simons *et al*., 1991; Golomb *et al*., 2004). Each NMHC can be divided into several structurally defined domains, with the molecular activities of the molecule being distributed among the different domains (reviewed in Warrick and Spudich, 1987; Bresnick, 1999; Conti and Adelstein, 2008). The N-terminal portion of the NMHC peptide forms a globular head, which is also referred to as the motor domain because it harbors the ATPase- and actin-binding activities of the molecule. The ELC and RLC associate with the heavy chains via interaction with IQ motifs that reside near the C-terminal end of the globular head, in a region often referred to as the neck domain. After the neck domain is an α-helical coiled-coil rod/tail domain, which mediates heavy chain homodimerization and filament assembly, and the molecule terminates with a nonhelical tailpiece (NHT) of ~34–44 amino acids (see Figure 4A).

All three myosin II isoforms are thought to perform the same two basic functions at the molecular level, namely, assembly into bipolar filaments and contraction of F-actin in an ATP-dependent manner (Conti and Adelstein, 2008). These molecular functions of myosin II are regulated in multiple ways. Perhaps the most well characterized mechanism of myosin II regulation is phosphorylation of the RLC at Ser19 (and to a lesser extent Thr18). RLC phosphorylation leads to both stimulated actin-activated ATPase activity and increased filament assembly (Tan *et al*., 1992; Bresnick, 1999). One of the key enzymes regulating the phosphorylation status of the RLC is Rho kinase (ROCK), which can directly phosphorylate the RLC as well as phosphorylate and inactivate the targeting subunit of the myosin light chain phosphatase (Amano *et al*., 1996; Kimura *et al*., 1996). Besides RLC phosphorylation, structural domains identified within the C-terminal portion of the myosin II tail, as well as protein

This article was published online ahead of print in *MBC in Press* (http://www.molbiolcell.org/cgi/doi/10.1091/mbc.E08–05–0533) on October 8, 2008.

* Present address: Department of Zoology, University of Wisconsin, Madison, WI 53706.

Address correspondence to: Anthony R. Means (means001@mc.duke.edu).

Abbreviations used: IIA and IIB, nonmuscle myosin II isoforms A and B; ACD, assembly competent domain; FRAP, fluorescence recovery after photobleaching; mChe, mCherry; NHT, nonhelical tailpiece; ROCK, Rho kinase; RLC, myosin regulatory light chain; TX-100, Triton X-100.

binding and phosphorylation events occurring within this region of the polypeptide, are also involved in regulation of myosin II filament assembly (Straussman *et al*., 2001; Dulyaninova *et al*., 2005; Nakasawa *et al*., 2005; Rosenberg *et al*., 2008).

Interestingly, although IIA and IIB perform the same molecular functions, specific depletion of these isoforms results in distinct migratory phenotypes. For example, specific depletion of IIA in various cell types results in increases in protrusive activity with concomitant increases in motility rates, whereas distinct, even opposing effects on migration occur with IIB depletion (Sandquist *et al*., 2006; Even-Ram *et al*., 2007). Thus, more than just regulating myosin II functions in general, cells can regulate myosin II functions in isoform-specific ways. One distinction between IIA and IIB that has been observed in motile cells is a difference in their subcellular distribution. Particularly, IIA is commonly found to enrich in the front of migrating cells relative to IIB, whereas IIB generally accumulates in the cell rear (Kolega, 1998; Saitoh *et al*., 2001; Kolega, 2003). This differential localization suggests that the spatiotemporal regulation of the activities of the different myosin II isoforms may contribute to their distinct functions in cell motility. However, the molecular mechanisms underlying isoform-distinct subcellular distributions in migrating cells are not well defined. Accordingly, we used a chimeric analysis to determine which region of the myosin heavy chain is responsible for directing isoform-specific distribution. Experimental analysis with the chimeras revealed that the predominant factor directing isoform-specific distribution is a small C-terminal region in the tail of the myosin heavy chain, a region that is responsible for regulating filament assembly. Swapping this domain between isoforms inverted several isoform-specific properties, demonstrating the importance of this domain in controlling the distinct functions of IIA and IIB. The results presented here thus advance our understanding as to how each isoform uniquely functions during the motile process.

MATERIALS AND METHODS

Antibodies and Reagents

Polyclonal antibodies for nonmuscle myosin II heavy chain A (PRB-440P) and B (PRB-445P) were purchased from Covance Research Products (Princeton, NJ). Monoclonal anti-β-actin antibody (AC-15; A-5441) was purchased from Sigma-Aldrich (St. Louis, MO). Polyclonal myosin light chain 2 (3672) and polyclonal phospho-myosin light chain 2 (Ser19; 3671) antibodies were purchased from Cell Signaling Technology (Danvers, MA). Polyclonal anti-green fluorescent protein (GFP) antibody (sc-8334) was obtained from Santa Cruz Biotechnology (Santa Cruz, CA). Cy3-conjugated AffiniPure goat anti-rabbit immunoglobulin G (IgG) (111-166-003) and fluorescein-conjugated AffiniPure goat anti-mouse IgG (115-095-146) antibodies were purchased from Jackson ImmunoResearch Laboratories (West Grove, PA). Secondary antibodies used for quantitative detection of protein with the Odyssey infrared imaging system (Li-Cor Biosciences, Lincoln, NE) were IRDye 800-conjugated affinity-purified goat anti-rabbit IgG (611-132-122; Rockland Immunochemicals, Gilbertsville, PA) and Alexa Fluor 680-conjugated goat anti-mouse IgG (A21058; Invitrogen, Carlsbad, CA). Rhodamine-conjugated phalloidin (R415) and Alexa Fluor 350-conjugated phalloidin (A22281) were from Invitrogen. Y27632 (688000), racemic blebbistatin (203390), and jasplakinolide (420127) were purchased from Calbiochem (San Diego, CA). All other reagents not specified were purchased from Sigma-Aldrich.

Cell Lines and Culture Conditions

Because the primary goal of this study was to characterize how IIA and IIB assume distinct distribution in motile cells, we examined isoform distribution in wound migrating A549 cells, a cell type in which these isoforms have been shown to perform distinct functions in wound migration (Sandquist *et al*., 2006). However, a key feature of normal IIA and IIB distribution is a strong colocalization with actin stress fibers. Therefore, we also used a simian virus 40-transformed variant of WI-38 human lung fibroblasts, because these cells form actin stress fibers more robustly than A549 cells and also undergo wound migration. We observed similar results for both cell types in our experiments; thus, the results for only one cell type are shown in each figure, as indicated in the figure legends. The A549 cells were maintained in Dulbecco's modified Eagle's medium supplemented with 10% heat-inactivated fetal bovine serum (FBS), and WI-38 cells were maintained in Eagle's minimal essential medium supplemented with 10% FBS. Both mediums included antibiotics (100 U/ml penicillin and 100 μg/ml streptomycin). All cells were cultured in a humidified atmosphere of 5% CO_2 at 37°C.

Transfections

A549 and WI-38 cells were transfected by nucleofection by using Cell Line Nucleofector lit T (VCA-1002) and kit R (VCA-1001), respectively, from Amaxa Biosystems (Gaithersburg, MD) by the suggested optimized protocol for each cell line, with the following exceptions. Nucleofection buffer consisted of 50 μl of Solution T or R, 50 μl of phosphate-buffered saline (PBS), and 11 μl of Supplement per 1×10^6 cells (A549) or 7.5×10^5 cells (WI-38), mixed immediately before nucleofection. For a single plasmid transfection, 3 μg of DNA was nucleofected per 1×10^6 cells, whereas 2 μg of DNA of each plasmid was used for cotransfection. After nucleuofection, the cells were directly plated into plastic 35-mm dishes and incubated overnight. Then, cells were trypsinized and replated appropriately for each of the assays described below. Experiments were generally conducted 24–36 h after replating.

Plasmids

GFP-IIA (Addgene plasmid 11347) and GFP-IIB (Addgene plasmid 11348) were obtained through Addgene (Cambridge, MA) and were originally described by Wei and Adelstein (2000). mChe-IIA and mChe-IIB were gifts from M. Vicente-Manzanares (Vicente-Manzanares *et al*., 2007). Note that the mChe-tagged constructs were derived by replacing the GFP from the above-mentioned constructs with mChe. Chimeric myosin IIs and deletion mutants were generated by swapping, or deleting, domains from the GFP-IIA and GFP-IIB constructs mentioned above. See Supplemental Data for a description of cloning procedures for construction of the chimeric and truncated myosin IIs.

Immunofluorescence

For immunofluorescence cells were grown on fibronectin-coated (20 μg/ml) glass coverslips. After the appropriate treatment, coverslips were washed with PBS and fixed by incubation in either 3% paraformaldehyde (PFA), 2% sucrose in PBS, pH 7.0, for 10–15 min, or ice-cold methanol for 20 min. PFA-fixed samples were permeabilized for 5 min in PBS containing 0.2% Triton X-100 (TX-100). For all samples, nonspecific binding sites were blocked for 15 min with blocking buffer (5% FBS in PBS containing 0.1% Triton X-100). Primary antibody binding was performed by either 1-h incubation at room temperature or overnight incubation at 4°C, with anti-IIA (1:200), anti-IIB (1:200), or anti-β-actin (1:500) antibodies diluted in blocking buffer, followed by a 1-h incubation at room temperature with the appropriate fluorochrome-conjugated secondary antibodies. Coverslips were mounted onto slides by using Prolong Antifade (P7481; Invitrogen).

Microscopy and Image Processing

Confocal images of fixed samples were obtained on an inverted Leica DMI60000CS with a conventional scanner and analyzed using Leica LAS AF software 1.7.0 (Leica Microsystems, Deerfield, IL). All other images of fixed samples were obtained using a Semrock Pinkel quadpass dichroic cube (440/520/606/699) on an upright AxioImager.A1 (Carl Zeiss, Thornwood, NY) coupled to a Orca ER monochrome cooled charge-coupled device (CCD) camera (Hamamatsu, Bridgewater, NJ) and analyzed with MetaMorph software release 7.5 (Molecular Devices, Sunnyvale, CA). For immunostaining of wound migrating cells, monolayers were wounded with the narrow end of a Cell Lifter (3008; Corning Life Sciences, Lowell, MA), and loose cells were washed off with PBS, followed by the addition of fresh media (phenol red free). Drug-treated samples were prepared as follows: wounded cells were allowed to migrate for 80 min, at which point the media were removed from the cells into a 15-ml tube and Y27632 (10 μM) or blebbistatin (100 μM) was added. The media plus drug were returned to the cells, which were then allowed to incubate and migrate for an additional 20 min before fixation.

For live cell time-lapse video microscopy, transfected A549 cells were trypsinized and replated onto fibronectin-coated (20 μg/ml) glass-bottomed microwell dishes (P35G-0-10-C; MatTek, Ashland, MA) and incubated for an additional 24–36 h before imaging. For wound healing migration, monolayers were wounded as mentioned above, and the wound edges were then scanned for cells expressing transfected protein. Images were obtained at the intervals indicated in the figure legends. For videos of drug-treated cells, to view the same cell before and after treatment, drug was added directly to cells on the microscope stage at a 3× concentration in a volume equal to half that already on the cells. Images were obtained of cells before and after treatment at the intervals indicated in the figure legends. All live cell time-lapse video microscopy was performed using a motorized Axio Observer Z1 (Carl Zeiss) housed in a Pecon XL S1 incubator to maintain samples at 5% CO_2 and 37°C and coupled to a CoolSNAP ES high-resolution CCD camera (Photometrics, Tucson, AZ). Images were acquired with a 40×/1.3 oil Plan-NeoFluar objective

and analyzed and processed using MetaMorph software release 7.5 (Molecular Devices).

Fluorescence Recovery after Photobleaching (FRAP)

Samples for FRAP experiments were prepared as described above for live cell time-lapse video microscopy. Confocal images for FRAP analysis were obtained on an inverted DMI60000CS (Leica Microsystems) with a conventional scanner and analyzed using LAS AF software 1.7.0 (Leica Microsystems). The microscope stand was housed in a Ludin cube to maintain the samples at 37°C. To image the FRAP, a cell expressing the GFP-tagged protein was first scanned three times to establish prebleach fluorescence intensity levels. A small region of the cell was then bleached with three scans at 100% laser power, followed by 30–40 subsequent scans at 3-s intervals to monitor FRAP. The bleached region was a circle of ~4 μm in diameter located near the periphery but not to the very cell edge. Thus, the bleached region was completely surrounded by GFP fluorescence signal such that recovery could occur from all around the bleached circle. The region bleached generally included GFP-tagged myosin II that occurred both as filamentous arrays (i.e., stress fibers) and as diffuse cytosolic protein. To correct for changes in fluorescence values due to cell movements or the bleaching associated with repeated scanning, intensity values in the bleached region were corrected against another region of similar initial intensity from a distant location within the same cell or a close neighbor cell. These corrected fluorescence intensity values were then normalized to the initial value, plotted versus time and fitted by a single exponential equation using Prism 4 (GraphPad statistical software; GraphPad Software, San Diego, CA), from which values for maximal percent recovery and half-life (i.e., time to half-maximal recovery) were determined.

Triton X-100 Solubility Assay

For untreated and drug treated samples in Figure 5, 5×10^5 A549 cells were plated and incubated for 24 h before treatment. Cells were treated with 10 μM Y27632 or 100 μM blebbistatin for 20 min before lysis. For transfected samples in Figure 5, nucleofected A549 cells (described above) were trypsinized and replated into 35-mm plastic dishes and incubated for an additional 24–36 h. Cells were generally 70–80% confluent at the time of lysis. Lysis for all samples was performed in the following manner: after washing the cells with ice-cold PBS, 100–150 μl of ice-cold buffer X (50 mM Tris-HCl, pH 7.5, 100 mM NaCl, 50 mM KCl, 5 mM $MgCl_2$, 2 mM dithiothreitol, 0.5% Triton X-100, and 1 μM microcystin, plus protease inhibitors) were added, and the cells were incubated in buffer X for 10 min on ice. Next, the cell lysates were collected by scrapping into 1.5-ml polyallomer microfuge tubes (357448; Beckman Coulter, Fullerton, CA), and the Triton X-100–soluble and –insoluble fractions were separated by centrifugation at ~90,000 $\times$ *g* for 10 min at 4°C. After centrifugation, the supernatant (soluble fraction) was removed from each tube, leaving behind the Triton X-100 insoluble pellet, and it was replaced with an equal volume of 2× SDS-sample buffer. The total protein concentrations of the supernates were determined using a DC protein assay (500-0116; Bio-Rad, Hercules, CA), and the supernates were then diluted to the desired final concentration with 3× SDS-sample buffer, being sure to dilute the paired insoluble pellets with the same volume. Finally, the samples were sonicated, to solubilize the pellets, and boiled for 10 min.

Equal volumes of insoluble and soluble fractions were separated by SDS-polyacrylamide gel electrophoresis (PAGE) with 6% polyacrylamide gels (Figure 5, to separate endogenous from tagged heavy chains) or with gels that were 10% in the top half and 15% in the bottom half, to separate both heavy and light chains. Quantitative immunoblotting was performed using the Odyssey infrared imaging system. In Figure 5, A and B, GFP-tagged wild-type and chimeric myosin IIs were first detected by immunoblotting for GFP, followed by stripping and reprobing for endogenous myosin IIs. For detection the fluorescence-labeled secondary antibodies described above were used. Quantification of the fluorescence signal associated with the immunoreactive bands was performed with Odyssey software version 1.2, except for total RLC (tRLC) and RLC phosphorylated at Ser19 (pRLC-S19). Immunoblots of tRLC and pRLC-S19 were exposed to film, and the immunoreactive bands were scanned and quantified by densitometry using Odyssey software. The Triton X-100 solubility of a particular protein was determined by dividing the signal of that protein in the soluble fraction by the sum of the signals of that protein in the soluble and insoluble fractions.

Data Analysis

Analysis of Triton X-100 solubility data was performed using StatView 5.0.1 (SAS Institute, Cary, NC). Values shown represent mean ± SEM from at least three experiments. Differences were analyzed first by analysis of variance (ANOVA), followed by Fisher's protected least significant difference to make pairwise comparisons. FRAP data were analyzed by two methods. First, the FRAP data were fit to single exponential growth equation using Prism 4 (GraphPad Software). The recovery curves shown in Figure 6 represent the average from 10 to 15 cells, treated as individual replicates. Using Prism 4 the maximal percentage of recovery (Y-max) and half-life, shown as mean ± SEM, were calculated for each recovery curve. The curves were compared using an F-test, whereas the Y-max and half-life values for each curve were compared using a Student's *t* test. As a second method to compare the recovery curves we performed an analysis of covariance (ANCOVA) by using StatView. For ANCOVA, the recovery curves were linearized by dropping the first three and last three time points and then making the reciprocal plot (i.e., 1/[percentage of recovery] vs. 1/[time]). For all tests, significance was assumed at $p < 0.05$.

RESULTS

IIA and IIB Exhibit Isoform-distinct Distribution in Migrating Cells

In our characterization of isoform-specific distribution, we wanted to directly compare the subcellular localization of IIA and IIB in the same cell. However, because the available isoform-specific antibodies for IIA and IIB are each produced in rabbit, we made use of GFP-tagged myosin IIs. The GFP-myosin IIs have been shown to colocalize with actin stress fibers similarly to endogenous proteins, as well as to rescue loss-of-function phenotypes associated with depletion of endogenous proteins (Wei and Adelstein, 2000; Bao *et al*., 2005; Vicente-Manzanares *et al*., 2007). Moreover, because the primary goal of this study was to characterize how IIA and IIB assume distinct distribution in motile cells, we examined isoform distribution in wound migrating cells.

Figure 1 shows images of WI-38 fibroblast cells expressing GFP-IIA or GFP-IIB that were fixed while undergoing wound migration and stained with isoform-specific antibodies for IIB or IIA, respectively. These images demonstrate that the isoform-distinct distribution of IIA and IIB in WI-38 cells is consistent with previous descriptions of the distribution of these isoforms in migrating endothelial and fibroblast cells (Kolega, 1998; Saitoh *et al*., 2001). In summary, IIA and IIB were each observed to distribute as puncta throughout the cell, and these puncta were often found to organize into linear arrays that coincided with actin filaments. Although both isoforms could be found to distribute as linear arrays of puncta, this filamentous appearance was much more pronounced with IIB (Figure 1, compare nontransfected cells marked with asterisks). Moreover, although both isoforms occupied central regions of cells, IIA was consistently found to distribute more anteriorly into protrusions than IIB (Figure 1, A and B, arrowheads), although there was generally observed a region at the very leading edge of the protrusion that was devoid of all myosin II but contained actin (Figure 1E, arrows). Importantly, GFP-IIA and GFP-IIB each distributed in a manner highly similar to its endogenous counterpart, and whether comparing GFP-IIB to endogenous IIA (Figure 1A) or GFP-IIA to endogenous IIB (Figure 1B), signal for IIB was consistently observed to be restricted relative to IIA such that a region existed toward the front of the cell where only IIA was detected.

We also examined the dynamics in the relationship between IIA and IIB in moving cells. To do so, we cotransfected A549 cells with both IIA that was tagged with the red fluorescent protein mCherry (mChe-IIA) and GFP-IIB, and we monitored their distribution relative to each other by time-lapse video microscopy of wound migrating cells. Figure 2 (also see Supplemental Video 1) shows that shortly after wounding, before the cells began to migrate, mChe-IIA and GFP-IIB significantly overlapped in their distributions, as noted by the yellowing in the merged images. However, as the cells began to protrude membrane into the wound the yellowing diminished, and the isoforms began to demonstrate differences in distribution, with mChe-IIA distributing more distally into the advancing protrusion than GFP-IIB, but again not to the extreme leading edge of the cells. Furthermore, the size of the mChe-IIA enrichment zone was dynamic. For example, in the cell on the right shown in

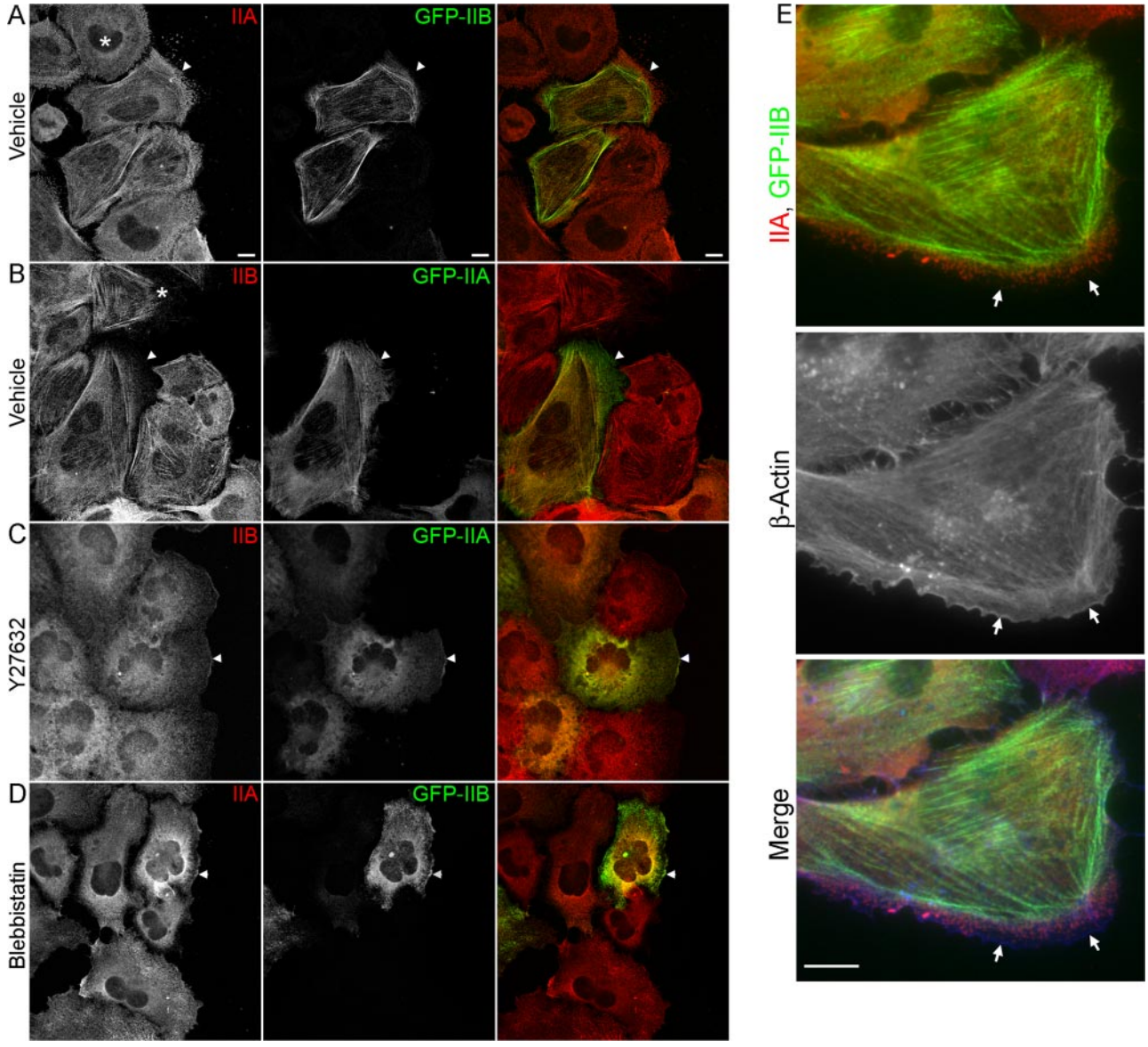

Figure 1. Y27632 and blebbistatin disrupt IIA and IIB distribution. (A–D) A monolayer of GFP-IIA– or GFP-IIB–expressing WI-38 cells was wounded and allowed to migrate for 60 min. The cells were then treated with vehicle (dimethyl sulfoxide), 10 μM Y27632, or 100 μM blebbistatin and incubated for an additional 20 min. After incubation, the cells were fixed with ice-cold methanol and stained with antibodies specific for the isoform not being expressed (shown in red). Normally, IIA distributed more anteriorly than IIB in migrating cells (arrowhead), whereas treatment with Y27632 or blebbistatin resulted in both isoforms acquiring a similarly diffuse distribution that extended to the leading edge. Asterisks (*) indicate nontransfected cells, which demonstrate the increased tendency of IIB puncta to form linear arrays compared with IIA. Bar, 10 μm. (E) Same as above, except the cells were also stained with an antibody to β-actin (blue). Arrows indicate regions of leading edge that are devoid of myosin II but contain actin. Bar, 20 μm.

Figure 2, mChe-IIA and GFP-IIB were observed to briefly overlap in a small region at the front of the cell where protrusion was temporarily stalled, but then the two isoforms quickly separated again once protrusion resumed (Figure 2, arrows).

Myosin II Inhibitors Similarly Disrupt IIA and IIB Distribution

We next examined the distribution of the myosin II isoforms after treatment with the small molecule inhibitors of myosin II Y27632 (Amano *et al*., 1996) and blebbistatin (Limouze *et al*., 2004), because these drugs have been reported previously to disrupt the distribution of IIA and IIB in different ways (Kolega, 2003, 2006). Figure 1, C and D, demonstrates that after treatment of wound migrating, GFP-IIA– or GFP-IIB–expressing WI-38 cells with either Y27632 (10 μM) or blebbistatin (100 μM) for 20 min before fixation, both IIA and IIB were observed to distribute more diffusely throughout the entire cell, with the signals of the two isoforms largely overlapping, as indicated by the yellowing in the merged images. Of note, after Y27632 or blebbistatin treatment IIB was no longer restricted from anterior regions of the cells. These results demonstrate and confirm that upon treatment with either Y27632 or blebbistatin, IIA and IIB no longer exhibit distinct distribution at the front of migrating cells.

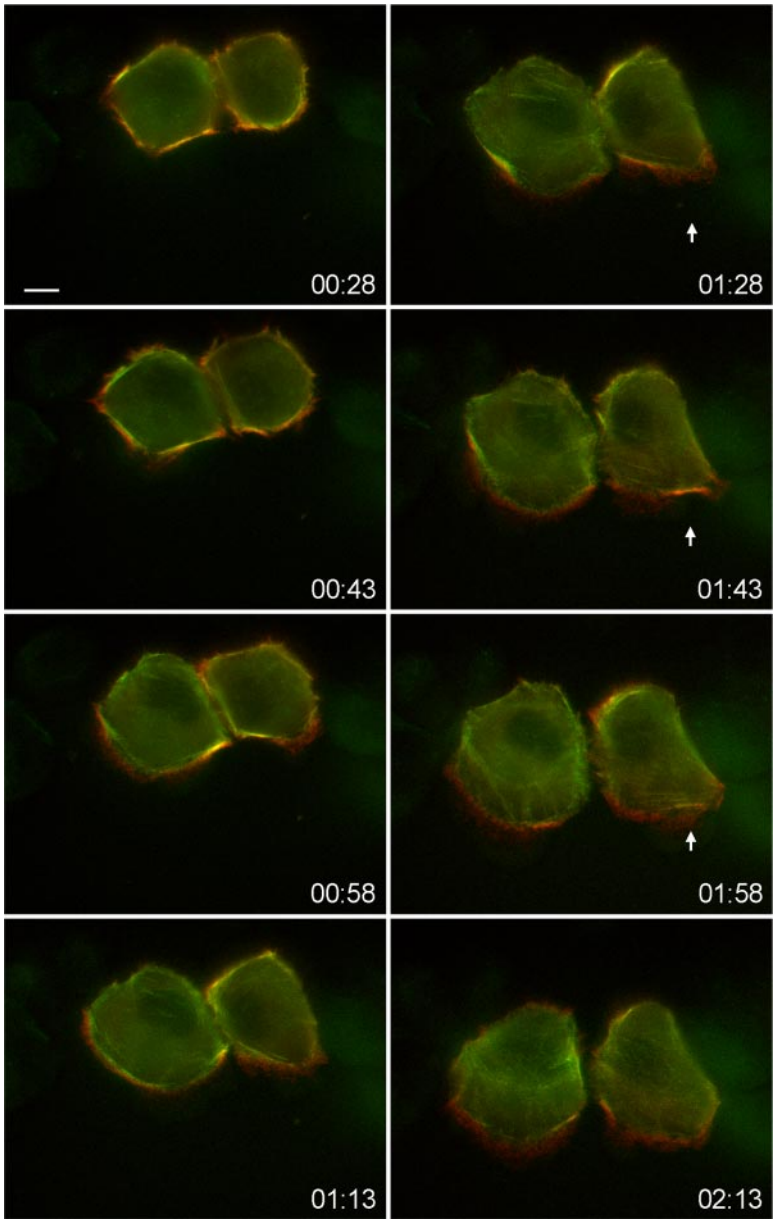

Figure 2. Still images from a time-lapse video of wound migration of A549 cells expressing mCherry-IIA (red) and GFP-IIB (green). This sequence is taken from Supplemental Video 1. Numbers in the bottom-right corner of the images indicate time after wounding (hh:mm). This sequence demonstrates that early after wounding IIA and IIB overlap in their distribution, but once protrusions begin to form IIA quickly acquires a more anterior distribution than does IIB, as noted by the formation of a zone of red signal near the front of the cell. Arrowheads indicate a point in the migration where protrusion is temporarily stalled and IIA and IIB distribution strongly overlaps again until the protrusion recommences.

We also used time-lapse video microscopy to examine the dynamics of the Y27632-induced disruption of IIA and IIB localizations in live cells. These videos demonstrate that, before treatment with Y27632, GFP-IIA and GFP-IIB were observed to form into filamentous arrays, similar to fixed cells (Figure 3 and Supplemental Videos 2 and 3). However, within minutes of addition of Y27632 the punctate, linear arrays of GFP-IIA and GFP-IIB were lost, with both isoforms rapidly becoming diffusely distributed throughout the entire cell. Furthermore, the sequence in Figure 2C clearly demonstrates that the Y27632-induced redistribution of GFP-IIB into regions of the cell from which it was formerly restricted shared a tight temporal relationship with loss of GFP-IIB from organized, linear arrays (Figure 3C, arrowheads). Live imaging of blebbistatin-treated cells was not performed due to the reported photosensitivity of this compound (Kolega, 2004). The data presented above demonstrate that inhibition of myosin II motor activity by two distinct mechanisms results in loss of the differential localizations of IIA and IIB, with both isoform becoming diffusely distributed.

The C Terminus of the Myosin Heavy Chain Directs Isoform-specific Distribution

Myosin II is a large molecule characterized by multiple structural domains, each of which performs a unique molecular function. Accordingly, we next sought to determine which domain(s) within the myosin II molecule directs isoform-specific distribution. To do so, we made chimeras of IIA and IIB in which different functional domains were swapped between them. For example, the chimera GFP-IIA-Btail consists of the globular head of IIA (amino acids 1-781) fused in frame to the neck and "tail" portion of IIB at the corresponding residue (amino acid 789 of IIB) such that the overall structure of the heavy chain remains intact (Figure 4A). This chimera thus harbors the actin binding and AT-

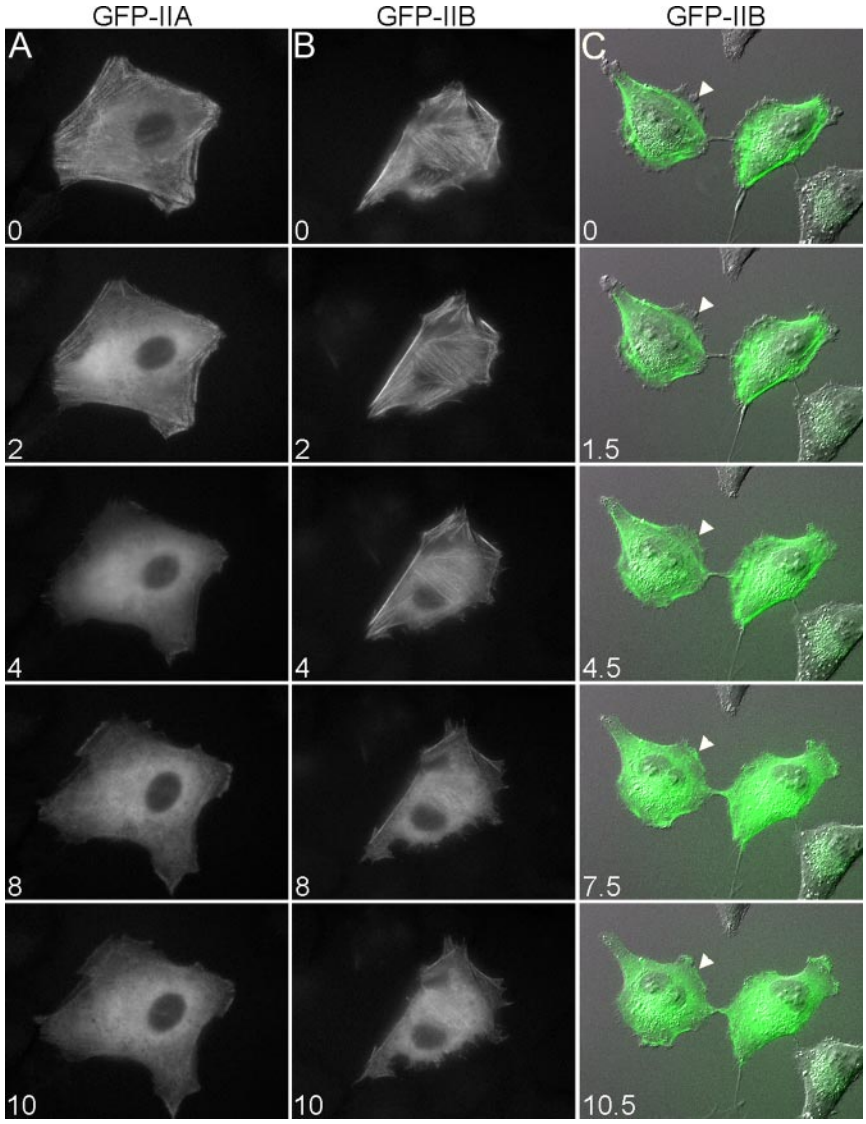

Figure 3. Still images from time-lapse videos demonstrate the effects of Y27632 treatment on the distribution of GFP-tagged myosins. Time-lapse videos of GFP-IIA (A) and GFP-IIB (B and C) expressing A549 cells were obtained before and after addition of 10 μM Y27632. Numbers in the bottom-left corner of the images indicate time in minutes after addition of drug. In C, differential interference contrast images are overlaid with the fluorescence images of GFP-IIB (green). This sequence demonstrates that after treatment with Y27632 GFP-IIB rapidly redistributes from organized, linear arrays into regions of the cell from which it was formerly restricted (arrowheads). The sequences shown in A and (B) are from Supplemental Videos 2 and 3, respectively. Bar, 20 μm.

Pase domains of IIA and the IQ motifs (light chain binding) and helical tail of IIB (Figure 4A).

Characterization of the distribution of GFP-IIA-Btail, together with that of the inverse chimera, should enable the assessment of the importance of the different enzymatic properties of IIA and IIB (Kovacs *et al*., 2003; Wang *et al*., 2003) in directing isoform-specific distribution. In particular, we reasoned that if motor activity is the main factor driving isoform-specific localization, then GFP-IIA-Btail, when expressed in WI-38 cells, would distribute in a manner most similar to endogenous IIA, and vice versa for the inverse chimera. Interestingly, Figure 4B shows that GFP-IIA-Btail distributed in wound migrating WI-38 cells in a manner very similar to IIB; that is, GFP-IIA-Btail was restricted from more anterior regions of the protrusion compared with endogenous IIA (Figure 4B, top row). Inversely, the chimera GFP-IIB-Atail was enriched over IIB in anterior regions of migrating cells, as noted by the region of bright green signal in the cell front (Figure 4B, bottom row). These results suggest that the domain responsible for directing isoform-specific localization is located within the neck and/or tail portion of the myosin heavy chain.

To more narrowly define which region of the myosin heavy chain directs isoform-specific localization, we generated chimeras of IIA and IIB in which only a small portion of the extreme C terminus of the myosin heavy chains were swapped (Figure 4A). This extreme C-terminal region of the myosin heavy chain (henceforth C-terminal region) contains several elements known to be important in regulating filament assembly, including one of two described assembly competent domains (ACDs), from which these chimeras derive their names (Nakasawa *et al*., 2005). As shown in Figure 4C, the chimera GFP-IIA-Bacd distributed similarly to both GFP-IIB and GFP-IIA-Btail in that it was restricted from protrusions compared with endogenous IIA (Figure 4C, top row). In contrast, GFP-IIB-Aacd acquired a more anterior distribution than endogenous IIB in the inverse comparison (Figure 4C, bottom row). Additionally, when GFP-IIA-Bacd and GFP-IIB-Aacd were expressed in cells in which the levels of endogenous IIB or IIA, respectively, were reduced by treatment with isoform-specific small interfering RNA, the chimeras still seemed to distribute normally (Supplemental Figure S1). These results suggest that the chimeras do not require the presence of their endogenous counterpart

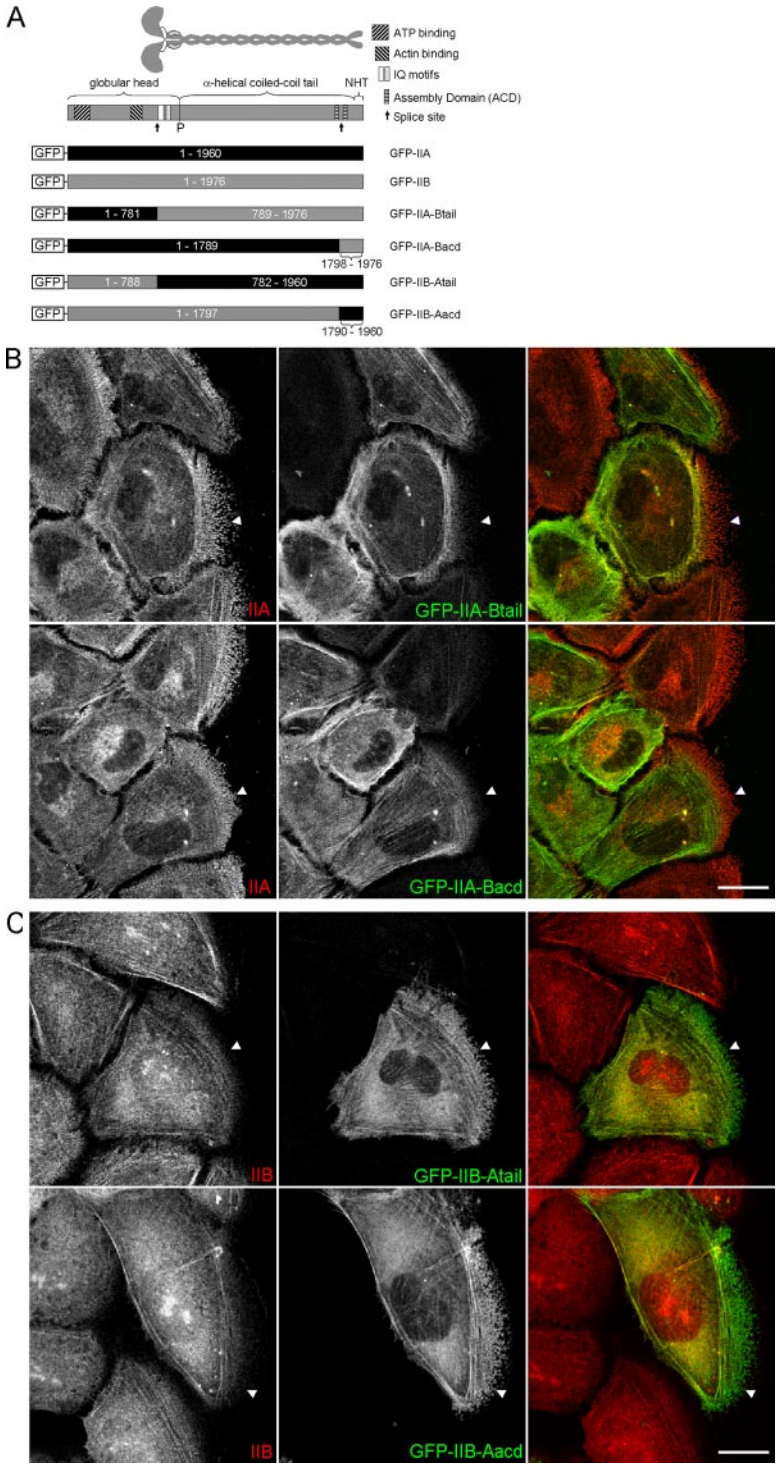

Figure 4. The C-terminal region of the myosin heavy chain regulates isoform-specific distribution. (A) Diagram depicting the domain structure of myosin II and the chimeras of IIA and IIB that were generated. The "P" indicates the position of the proline residue that is commonly used to mark the beginning of the helical tail. NHT, nonhelical tailpiece. (B and C) Confocal images of wound migrating WI-38 cells expressing the indicated chimeras. In all images the cells are migrating to the right. The cells were fixed 90 min after wounding and immunostained with antibodies specific for the isoform opposite the tail portion of the chimera so that the antibody would only detect endogenous protein (red, as indicated in the images). Arrowheads serve as reference points showing the more anterior distribution of IIA and chimeras with the IIA-tail or -acd. Bar, 20 μm.

to function, but rather they possess the intrinsic ability to distribute properly.

Last, similar to what was done in Supplemental Video 1, we used time-lapse video microscopy to compare the localization of GFP-IIA-Bacd to mChe-IIA in live cells. Supplemental Video 4 demonstrates that GFP-IIA-Bacd and mChe-IIA distribute relative to one another in migrating cells in a manner highly similar to that of GFP-IIB and mChe-IIA. Specifically, GFP-IIA-Bacd was restricted in distribution compared with mChe-IIA. Together the data presented in this section strongly support the idea that the C-terminal region, and not the motor domain, is the main factor directing the isoform-distinct distribution of IIA and IIB.

The C-Terminal Region Regulates Isoform-distinct Solubility

The C-terminal region previously has been shown to play important roles in the regulation of myosin II filament assembly (Dulyaninova *et al.*, 2005; Rosenberg *et al.*, 2008). Therefore, we next evaluated whether a correlation exists

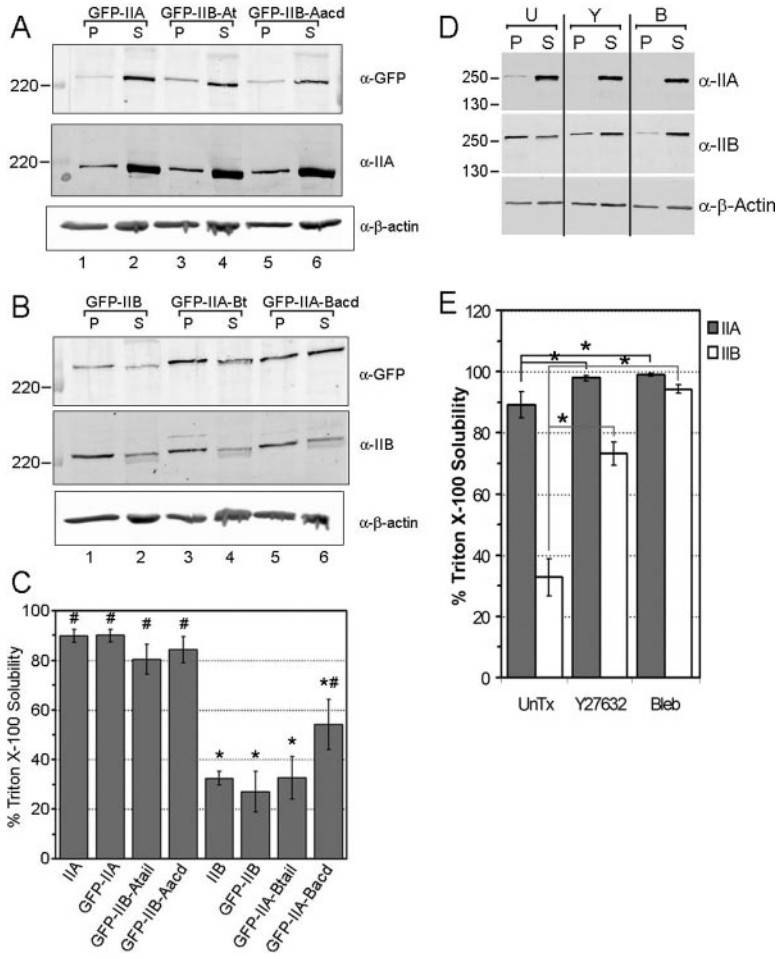

Figure 5. The C-terminal region regulates isoform-specific assembly properties. (A) Representative immunoblots TX-100–insoluble pellet (P) and soluble (S) fractions of lysates from A549 cells expressing GFP-IIA or the indicated chimeras. The amount of the transfected forms of myosin II purifying in equivalent amounts of insoluble and soluble fractions were first detected using an antibody against GFP (top), then the membrane was stripped and reprobed with an antibody specific for IIA to detect the endogenous IIA (middle). (B) Same as in A, except for GFP-IIB and the indicated chimeras. Note the GFP-tagged forms of myosin II are weakly detected as slower running bands (middle), indicating the low transfection efficiency of these proteins. (C) Bar graph demonstrating the percent solubility (see *Materials and Methods*) of each form of myosin II, endogenous and transfected, represented as mean ± SEM from three identical experiments. Asterisk (*) indicates a statistical difference from GFP-IIA, whereas number sign (#) indicates a statistical difference from GFP-IIB, with a p value <0.05. (D) Representative immunoblots of TX-100–insoluble and –soluble fractions of untreated (U) A549 cell lysates or after treatment with 10 μM Y27632 (Y) or 100 μM blebbistatin (B) for 20 min before lysis. The antibodies used for immunoblotting are shown on the right, whereas the positions of several molecular weight markers (kilodaltons) are indicated on the left. (E) Bar graph demonstrating the percent solubility of each isoform after the various treatments, represented as mean ± SEM from five identical experiments. Asterisk (*) indicates a statistical difference from untreated sample at a p value <0.05.

between the specific assembly properties and distribution of IIA, IIB, and the chimeras. The TX-100 solubility assay has been used as an indicator of the in vivo assembly state of myosin II (Ben-Ya'acov and Ravid, 2003). In this assay, TX-100 cell lysates are separated into soluble and insoluble fractions by high-speed centrifugation. The filamentous myosin II in the cell is associated with the actin cytoskeleton and partitions with the insoluble pellet, whereas unassembled myosin II monomers remain in the soluble supernatant. We expressed the GFP-tagged forms of IIA, IIB, and the chimeras in A549 cells and we compared the TX-100 solubility of each transfected myosin II with those of the endogenous isoforms. The results of the TX-100 assay demonstrate that ~89% of IIA partitions in the soluble fraction regardless of what form of GFP-tagged myosin II is expressed (Figures 5A, middle, and 5C), whereas the TX-100 solubility of IIB is ~32% (Figures 5B, middle, and 5C). Importantly, the TX-100 solubilities of endogenous IIA and IIB in transfected cells are identical to the solubilities of these isoforms in nontransfected, untreated cells (compare IIA and IIB in Figure 5C with untreated [U] samples in Figure 5D). Finally, the average TX-100 solubilities of both GFP-IIA and GFP-IIB are similar to those of their endogenous counterparts (Figure 5C).

We next characterized the TX-100 solubility of the chimeras. As shown in Figure 5, the average TX-100 solubilities of GFP-IIB-Atail and GFP-IIB-Aacd, 80 and 84%, respectively, were each highly similar to GFP-IIA and significantly greater than GFP-IIB. The inverse comparison revealed a similar result, with GFP-IIA-Btail and GFP-IIA-Bacd both exhibiting solubility in TX-100 most similar to GFP-IIB. Moreover, the average solubilities of GFP-IIA-Btail and GFP-IIA-Bacd, 33 and 54%, respectively, were both significantly less than that of GFP-IIA, whereas the later was also significantly different from GFP-IIB (Figure 5C). These data demonstrate that the C-terminal region regulates the TX-100 solubility of, and by extension the fraction of monomeric versus filamentous, IIA and IIB in an isoform-specific manner. Furthermore, they reveal a correlation between solubility and subcellular distribution for IIA, IIB, and the chimeras. Specifically, the forms of myosin II that are more soluble in TX-100, GFP-IIA, GFP-IIB-Atail, and GFP-IIB-Aacd, distribute more anteriorly in migrating cells, whereas the less TX-100–soluble forms, GFP-IIB, GFP-IIA-Btail, and GFP-IIA-Bacd, assume a more restricted distribution.

Finally, because Y27632 and blebbistatin treatments disrupted normal IIA and IIB distribution (Figures 1 and 3), we examined the effects of these drugs on the TX-100 solubility of the two myosin II isoforms. Figure 5D shows that treatment of cells with 10 μM Y27632 or 100 μM blebbistatin for 20 min before lysis resulted in a significant increase in the TX-100 solubility of each isoform, but to different extents. Specifically, the average TX-100 solubility of IIA increased from 89% in untreated cells to 97 or 98% in Y27632- or blebbistatin-treated cells, respectively (Figure 5, D and E). In contrast, ~73 and 89% of cellular IIB purified in the supernatants of Y27632- or blebbistatin-treated cells, respectively, up from 35% in the untreated cells. That Y27632 increases

the TX-100 solubility of IIA and IIB is consistent with the idea that phosphorylation of the RLC modulates the assembly properties of myosin II (Trybus, 1991; Tan *et al*., 1992). Interestingly, although the TX-100 solubility of IIB after treatment with either drug is significantly greater than the untreated sample, the solubility of IIB in Y27632 or blebbsitatin is also significantly different from each other. The above-mentioned finding that both drugs significantly increase the solubilities of IIA and IIB is consistent with the observation that both drugs result in a more diffuse distribution of IIA and IIB (Figures 1 and 3).

The C-Terminal Region Dictates the In Vivo Mobilities of IIA and IIB

The results presented above reveal a correlation between the solubility and subcellular distribution of IIA and IIB, which is mediated through the C-terminal region. Furthermore, Supplemental Video 1 demonstrates that IIA more rapidly redistributes into newly formed protrusions than does IIB. Because monomers of myosin II are relatively more mobile than filamentous myosin II, the assembly state of a pool of myosin II, i.e., the ratio of monomeric versus filamentous myosin II, is predicted to directly impact its mobility. Accordingly, we next characterized the kinetics of the movements of IIA, IIB, and the chimeras within the cell by using FRAP. Figure 6 demonstrates that both the rate and extent of GFP-IIA turnover in A549 cells are greater than those of GFP-IIB. Specifically, the GFP-IIA fluorescence signal within the bleached region recovered to ~74% of the prebleach intensity, with an average time to half-maximal recovery, or half-life, of ~31 s, whereas GFP-IIB exhibited a recovery of ~60% with a half-life of 39 s. The differences in the FRAP of GFP-IIA and GFP-IIB shown here are consistent with previous reports (Vicente-Manzanares *et al*., 2007).

We next performed FRAP experiments with GFP-IIB-Aacd and GFP-IIA-Bacd to determine how swapping the C-terminal regions between IIA and IIB affects the turnover properties of each isoform. Figure 6 shows that the rate and extent of GFP-IIB-Aacd turnover were greater than those of GFP-IIA-Bacd. Moreover, the relationship between the recovery curves of GFP-IIB-Aacd and GFP-IIA-Bacd was very similar to the relationship between the recovery curves of GFP-IIA and GFP-IIB (Figure 6; compare the relationship between the two gray curves to the relationship between the two black curves). Thus, swapping the C-terminal regions between isoforms inverted the normal turnover properties of GFP-IIA and GFP-IIB. Interestingly, when the turnover properties of GFP-IIB-Aacd were compared with those of GFP-IIA, the extent of turnover for the two molecules was similar, whereas the half-life of the chimera was shorter than that of the wild-type molecule (Figure 6). A similar relationship was noted for GFP-IIA-Bacd and GFP-IIB. Nevertheless, these results indicate that the overall turnover properties of GFP-IIA and GFP-IIB-Aacd are more dynamic than those of GFP-IIB and GFP-IIA-Bacd, respectively.

Finally, when we examined the FRAP of truncation mutants of IIA and IIB in which the C-terminal region had been deleted, GFP-IIAΔacd and GFP-IIBΔacd, respectively, they were found to exhibit nearly identical turnover properties to each other (Figure 6). Specifically, both of these Δacd-mutants recovered very rapidly to ~90% of prebleach values. Moreover, the turnover properties of GFP-IIA and GFP-IIB in the presence of Y27632 were similar to both each other and the Δacd-mutants. These latter results demonstrate that under conditions where IIA and IIB are predicted to not form filaments, such as in the presence of Y27632 or due to deletion of the C-terminal region (Supplemental Figure 2), the two isoforms no longer exhibit unique turnover properties.

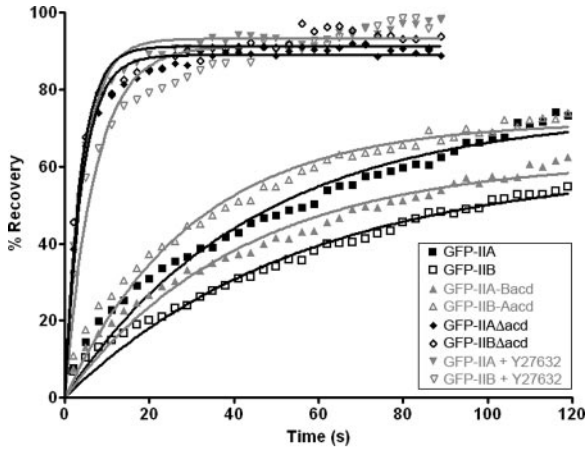

	Y-max (%Recovery)		Half-Life (s)	
	Mean	SEM	Mean	SEM
GFP-IIA	74#	1.9	31#	1.9
GFP-IIB	60*	0.7	39*	2.3
GFP-IIA-Bacd	62*	1.9	29#	2.3
GFP-IIB-Aacd	72#	1.5	21*#	1.4
GFP-IIA + Y27632	93*#	0.5	3.0*#	0.13
GFP-IIB + Y27632	91*#	0.6	4.9*#	0.20
GFP-IIAΔacd	89*#	0.6	2.8*#	0.17
GFP-IIBΔacd	91*#	0.6	2.6*#	0.16

Figure 6. The in vivo mobilities of IIA and IIB are dictated by their C-terminal regions. FRAP curves for various forms of myosin II. See *Materials and Methods* for a discussion on how FRAP analysis was performed. Briefly, A549 cells were transfected with one of the forms of myosin II, and an image of a GFP-positive cell was acquired before photobleaching to establish a baseline. After bleaching of a small region, images were acquired for 1.5–2 min at 3-s intervals to assess the recovery of the fluorescence signal in the bleached region. For Y27632-treated samples, GFP-IIA– or GFP-IIB–expressing cells were preincubated for 15 min with 10 μM Y27632, and then FRAP analysis was performed in the continued presence of the drug. The Δacd-mutans are described in the text. Individual points represent the mean values from 10 to 15 cells for each form of myosin II, and the points are fitted to a single exponential equation (lines), from which the maximal recoveries and half-lives are calculated (table). Asterisk (*) indicates a statistical difference from GFP-IIA, whereas number sign (#) indicates a statistical difference from GFP-IIB, with a p value <0.05.

DISCUSSION

Myosin II plays important roles in regulating a multitude of cellular activities, which contribute to a diverse array of biological processes. It is fascinating that for all the myosin II-dependent cellular activities that have been described, the basic molecular functions of myosin II are only two, namely, the assembly of monomers into filaments and ATPase-driven motor activity (Conti and Adelstein, 2008). How cells spatially and temporally regulate these two functions appropriately to orchestrate biological processes as different as cytokinesis and migration has long been a subject of scientific inquiry. In this study we sought to characterize how the isoform-distinct subcellular distribution of IIA and IIB seen in migrating cells is regulated, as this difference between the isoforms has been proposed to contribute to proper cell motility.

The results presented here demonstrate that the C-terminal region of the myosin heavy chain plays a primary role in directing isoform-specific distribution. This was a surprising finding because previous results suggested that the different motor activities of IIA and IIB led to their distinct localizations. For example, IIA is frequently observed to move faster and further into protrusions than IIB, and the former is known to exhibit higher motor activity than latter (Kelley *et al*., 1996). Moreover, IIA and IIB no longer exhibit distinct distribution in cells treated with small molecules that inhibit myosin II motor activity (Kolega, 2003, 2006). However, our observation that the chimera IIA-Bacd, a molecule that is ~91% IIA and 9% IIB by amino acid sequence, distributes in a manner highly similar to IIB, with the same being true for the inverse chimera, IIB-Aacd, strongly suggests that functions of the extreme C-terminal tail region supersede differences in motor activity in controlling isoform-specific distribution.

That the C-terminal region contributes to myosin II distribution in an isoform-specific manner should not be surprising, because within this region of the heavy chain the amino acid sequences of IIA and IIB diverge most significantly and protein binding and phosphorylation events occur that have been suggested previously to be important factors regulating myosin II distribution (Li and Bresnick, 2006; Rosenberg and Ravid, 2006). However, our chimeric data are the first to suggest that this region not only contributes to but also plays the primary role in determining how IIA and IIB distribute throughout a moving cell. It is important to note, however, that although IIA-Bacd is most similar to IIB in TX-100 solubility, turnover properties and subcellular distribution, the two are not identical. For example, although the TX-100 solubility of IIA-Bacd is closer to that of IIB than IIA, the solubility of the chimera was still significantly greater than that of IIB. One explanation for this is that the C-terminal region used here only includes one of two described ACDs (Nakasawa *et al*., 2005). Perhaps if the swapped regions were expanded slightly to include both of the ACDs, the similarities would be even greater. This supposition is supported by our observation that the chimera in which the larger region was swapped, IIA-Btail, functioned nearly identically to IIB.

Further evidence that a larger C-terminal region would induce the IIA-Bacd chimera to behave more like full-length IIB comes from studies examining the expression of IIB truncation fragments. For example, when expressed in cells, a fragment of the C-terminal portion of the IIB heavy chain that is slightly larger than, and fully encompasses, the C-terminal region used here was shown to disrupt the function of IIB, leading to cytoskeletal phenotypes similar to those that occur upon depletion of IIB (Sato *et al*., 2007). In contrast, when we expressed the C-terminal regions of IIA or IIB from this study in cells neither produced any obvious effects on cell morphology (data not shown), consistent with a previous report in which a similar, slightly smaller fragment of IIB was expressed in cells (Ben-Ya'acov and Ravid, 2003). Therefore, the C-terminal region from our study seems to impart isoform-specific function when in the context of a full-length chimera, but this region is not enough to disrupt the function of the full-length isoform when expressed as a fragment. Interestingly, in contrast to the discrepancy between IIA-Bacd and IIB, the chimera IIB-Aacd behaved very similarly to IIA. This may simply reflect that changes to the structure of the C-terminal region within the myosin heavy chain (i.e., swapping the domains between the isoforms) by default more easily lead to increases rather than decreases in solubility. Alternatively, IIB may be dually regulated by the C-terminal region and changes in RLC phosphorylation (see more on this topic below).

It is tempting to speculate as to how the C-terminal region regulates isoform-distinct distribution. One explanation is that in regulating each isoform's assembly into filaments, the different C-terminal regions of IIA and IIB control the pool of each isoform that is available to move into a new protrusion. Thus, when a new protrusion is formed in a migrating cell due to the extension of actin filaments, the nascent protrusion is temporarily devoid of myosin II until soluble myosin II molecules, filamentous myosin II being relatively stationary, redistribute there, although not to the very leading edge (Figure 1) because the compact nature of the actin meshwork in this region is thought to prohibit the movement of myosin II (DeBiasio *et al*., 1988). Because nearly 90% of the cellular pool of IIA, compared with ~30% of IIB, exists in the soluble fraction, the concentration gradient for the movement of IIA into the protrusion is larger than that of IIB. Furthermore, it is relevant to note that in each of the cells types used in this study there is greater than 500 times more IIA than IIB at the mass level, whereas smaller ratios were observed in other cell types (Supplemental Figure S3). However, whether the dramatically different levels of IIA and IIB observed in the cell types used here contribute to their unique distributions is not clear at this time.

The above-mentioned idea raises the question, How do soluble IIA and IIB redistribute into the protrusion? FRAP data shown here, as well as in previous studies (Kolega and Taylor, 1993), indicate that diffusion of soluble myosin II is quite rapid and could account for the movement of these molecules within the cell. For example, in Y27632-treated cells the fluorescence signals of both GFP-IIA and GFP-IIB recovered very rapidly and nearly completely after photobleaching. Moreover, the recovery curves of GFP-IIAΔacd and GFP-IIBΔacd, deletion mutants that lack the C-terminal region and thus the ability to assemble into filaments (Supplemental Figure S2), are highly similar to those of their full-length counterparts in the presence of Y27632. Thus, under conditions of decreased motor activity and/or decreased filament assembly IIA and IIB exhibit similarly rapid movement kinetics, consistent with the idea that diffusion of soluble, nonfilamentous molecules can account for rapid movements of these isoforms within the cell. However, because the diffusion rates of soluble IIA and IIB seem to be similar, diffusion alone cannot explain the enrichment of IIA over IIB in more anterior regions of protruding cells. So, because the diffusion rates of IIA and IIB are similar, if simple diffusion was the only factor then the ratio of IIA to IIB in the protrusion would be the same as the region from where they came. Thus, it is necessary to consider active movement as a mechanism of myosin II redistribution into protrusions, especially because diffusion of myosin II-sized molecules is limited in protrusions (Luby-Phelps *et al*., 1987). However, the differences in the motor properties of IIA and IIB do not seem to be what controls their distinct redistribution because IIB-Aacd and IIB harbor the same motor domain and the former distributes more anteriorly than does the latter.

With regard to this issue, it is our interpretation that the main factor directing the differential distribution of IIA and IIB is not how these isoforms move into the protrusion but rather how much of each is available to move. Accordingly, the FRAP experiments demonstrate that in untreated cells the turnover of IIA within a given region occurs more rapidly and to a greater extent compared with IIB. Therefore, under normal conditions when soluble IIA and IIB move into a newly formed protrusion, effectively decreasing the

amount of soluble IIA and IIB in the more posterior region, the re-equilibration of the ratio of filamentous to soluble IIA will be more rapid and occur to a greater extent than that of IIB in a given period. Thus, as IIA and IIB move out of the region directly posterior to the protrusion and into the protrusion, the pool of IIA in the more posterior region that is soluble and able to redistribute into the new protrusion will increase relative to IIB, facilitating the enrichment of IIA over IIB in the protrusion. A prediction from this model is that if protrusion ceases, IIB will eventually re-equilibrate with IIA in the protrusion. This prediction is supported by Figure 2 (also see Supplemental Video 1), in which mChe-IIA and GFP-IIB are observed to briefly overlap in a small region at the front of the migrating cell where protrusion is temporarily stalled, but then the two isoforms quickly separate again once protrusion is resumed.

Further support for the above-mentioned model can be found in previous studies demonstrating a correlation between myosin II assembly properties and distribution. In particular, a heavy meromyosin version of IIA, which dimerizes but does not form filaments, redistributes more quickly into protrusions than does full-length IIA (Kolega, 2006). Moreover, a recent study examining the role of charge distribution within the C-terminal region in regulating IIB filament assembly demonstrated a correlation between filament assembly and IIB localization (Rosenberg *et al*., 2008). Specifically, mutations of the charged regions in the C-terminal tail of IIB that decreased solubility in TX-100 relative to wild-type protein resulted in an increased tendency to accumulate in posterior regions of the cell, and vice versa for mutations that increased TX-100 solubility.

Although the primary role of the C-terminal region is thought to be regulation of assembly, we cannot rule out other ways in which this region could regulate isoform-specific distribution. For example, it is possible that as yet unidentified proteins selectively interact with the C-terminal region of IIA or IIB and shuttles or anchors the respective isoform to the appropriate cellular locale. Indeed, isoform-specific protein–protein interactions have been described to occur within this region. For example, the NHT of IIA exhibits a unique protein–protein interaction with the small calcium-binding protein S100A4 (Mts1), although the function of S100A4 binding also seems to be regulation of IIA assembly properties (Li and Bresnick, 2006).

We also cannot rule out a role for RLC phosphorylation in isoform distribution. For example, the chimera GFP-IIA-Btail, which harbors the IQ domains and C-terminal region of IIB, exhibits solubility in TX-100 more similar to IIB than does GFP-IIA-Bacd. Because RLC phosphorylation is known to impact myosin II filament assembly, the above-mentioned result may indicate that the regulation of IIB solubility is multifactorial, involving regulatory events occurring both at the C-terminal tail and at the RLC. Interestingly, results from a previous study suggested that IIA and IIB may be differentially regulated by ROCK (Sandquist *et al*., 2006). Moreover, it is shown here that Y27632 treatment increased the solubility of IIA and IIB to different extents, namely, IIA was nearly completely soluble after Y27632 treatment whereas ~25% of IIB remained insoluble under identical conditions. Thus, it is possible that tight spatiotemporal regulation of RLC phosphorylation within the cell may play a significant role in differential IIA and IIB distribution.

Conversely, it is perhaps not too surprising that the extent of the effect of Y27632 on the solubility of IIA and IIB is different considering the solubility of IIA in untreated cells is already much higher than that of IIB. However, the Triton-solubilities of IIA and IIB after blebbistatin treatment were much more similar, despite the basally higher level of IIA solubility. This discrepancy in the effects of Y27632 and blebbistatin is likely to reflect the fact that these drugs inhibit myosin II activity by different mechanisms. Y27632 decreases RLC phosphorylation via inhibiting ROCK, whereas blebbistatin directly binds ADP-bound myosin II, locking it in the low actin affinity state (Kovacs *et al*., 2004). That blebbistatin produces a similar effect upon IIA and IIB solubility is consistent with previous studies demonstrating that the actin binding properties of IIA and IIB are similar (Kelley *et al*., 1996; Kovacs *et al*., 2003) and that blebbistatin inhibits the MgATPase activity of both isoforms equivalently (Straight *et al*., 2003). The above-mentioned result thus serves as an important reminder that the solubility of myosin II in TX-100 may be modulated by more than just filament assembly but also by other factors such as specific binding to actin or even entrapment in actin networks. Clearly, much more work is needed to fully understand the mechanisms by which the C-terminal regions of IIA and IIB uniquely regulate the assembly of these isoforms, as well as how this region works in conjunction with phosphorylation, protein binding or other mechanisms yet to be discovered in regulating the differential distribution of IIA and IIB in migrating cells.

ACKNOWLEDGMENTS

We thank M. Vicente-Manzanares and A. F Horwitz (University of Virginia, Charlottesville, VA) for the gifts of the mChe-IIA and mChe-IIB plasmids. We are also grateful to K. Burridge (University of North Carolina, Chapel Hill, NC) and D. P Kiehart (Duke University, Durham, NC) for helpful discussion, and again to K. Burridge for critical reading of the manuscript. J. C. Sandquist is a Howard Hughes Medical Institute predoctoral fellow. This work was supported by National Institutes of Health grant CA-082845 (to A.R.M.).

REFERENCES

Amano, M., Ito, M., Kimura, K., Fukata, Y., Chihara, K., Nakano, T., Matsuura, Y., and Kaibuchi, K. (1996). Phosphorylation and activation of myosin by Rho-associated kinase (Rho-kinase). J. Biol. Chem. *271*, 20246–20249.

Bao, J., Jana, S. S., and Adelstein, R. S. (2005). Vertebrate nonmuscle myosin II isoforms rescue small interfering RNA-induced defects in COS-7 cell cytokinesis. J. Biol. Chem. *280*, 19594–19599.

Ben-Ya'acov, A., and Ravid, S. (2003). Epidermal growth factor-mediated transient phosphorylation and membrane localization of myosin II-B are required for efficient chemotaxis. J. Biol. Chem. *278*, 40032–40040.

Bresnick, A. R. (1999). Molecular mechanisms of nonmuscle myosin-II regulation. Curr. Opin. Cell Biol. *11*, 26–33.

Chrzanowska-Wodnicka, M., and Burridge, K. (1996). Rho-stimulated contractility drives the formation of stress fibers and focal adhesions. J. Cell Biol. *133*, 1403–1415.

Conti, M. A., and Adelstein, R. S. (2008). Nonmuscle myosin II moves in new directions. J. Cell Sci. *121*, 11–18.

DeBiasio, R. L., Wang, L. L., Fisher, G. W., and Taylor, D. L. (1988). The dynamic distribution of fluorescent analogues of actin and myosin in protrusions at the leading edge of migrating Swiss 3T3 fibroblasts. J. Cell Biol. *107*, 2631–2645.

Dulyaninova, N. G., Malashkevich, V. N., Almo, S. C., and Bresnick, A. R. (2005). Regulation of myosin-IIA assembly and Mts1 binding by heavy chain phosphorylation. Biochemistry *44*, 6867–6876.

Even-Ram, S., Doyle, A. D., Conti, M. A., Matsumoto, K., Adelstein, R. S., and Yamada, K. M. (2007). Myosin IIA regulates cell motility and actomyosin-microtubule crosstalk. Nat. Cell Biol. *9*, 299–309.

Golomb, E., Ma, X., Jana, S. S., Preston, Y. A., Kawamoto, S., Shoham, N. G., Goldin, E., Conti, M. A., Sellers, J. R., and Adelstein, R. S. (2004). Identification and characterization of nonmuscle myosin II-C, a new member of the myosin II family. J. Biol. Chem. *279*, 2800–2808.

Kelley, C. A., Sellers, J. R., Gard, D. L., Bui, D., Adelstein, R. S., and Baines, I. C. (1996). *Xenopus* nonmuscle myosin heavy chain isoforms have different subcellular localizations and enzymatic activities. J. Cell Biol. *134*, 675–687.

Kimura, K. *et al*. (1996). Regulation of myosin phosphatase by Rho and Rho-associated kinase (Rho-kinase). Science *273*, 245–248.

Kolega, J. (1998). Cytoplasmic dynamics of myosin IIA and IIB: spatial 'sorting' of isoforms in locomoting cells. J. Cell Sci. *111*, 2085–2095.

Kolega, J. (2003). Asymmetric distribution of myosin IIB in migrating endothelial cells is regulated by a rho-dependent kinase and contributes to tail retraction. Mol. Biol. Cell *14*, 4745–4757.

Kolega, J. (2004). Phototoxicity and photoinactivation of blebbistatin in UV and visible light. Biochem. Biophys. Res. Commun. *320*, 1020–1025.

Kolega, J. (2006). The role of myosin II motor activity in distributing myosin asymmetrically and coupling protrusive activity to cell translocation. Mol. Biol. Cell *17*, 4435–4445.

Kolega, J., and Taylor, D. L. (1993). Gradients in the concentration and assembly of myosin II in living fibroblasts during locomotion and fiber transport. Mol. Biol. Cell *4*, 819–836.

Kovacs, M., Toth, J., Hetenyi, C., Malnasi-Csizmadia, A., and Sellers, J. R. (2004). Mechanism of blebbistatin inhibition of myosin II. J. Biol. Chem. *279*, 35557–35563.

Kovacs, M., Wang, F., Hu, A., Zhang, Y., and Sellers, J. R. (2003). Functional divergence of human cytoplasmic myosin II: kinetic characterization of the non-muscle IIA isoform. J. Biol. Chem. *278*, 38132–38140.

Lauffenburger, D. A., and Horwitz, A. F. (1996). Cell migration: a physically integrated molecular process. Cell *84*, 359–369.

Li, Z. H., and Bresnick, A. R. (2006). The S100A4 metastasis factor regulates cellular motility via a direct interaction with myosin-IIA. Cancer Res. *66*, 5173–5180.

Limouze, J., Straight, A. F., Mitchison, T., and Sellers, J. R. (2004). Specificity of blebbistatin, an inhibitor of myosin II. J. Muscle Res. Cell Motil. *25*, 337–341.

Luby-Phelps, K., Castle, P. E., Taylor, D. L., and Lanni, F. (1987). Hindered diffusion of inert tracer particles in the cytoplasm of mouse 3T3 cells. Proc. Natl. Acad. Sci. USA *84*, 4910–4913.

Nakasawa, T., Takahashi, M., Matsuzawa, F., Aikawa, S., Togashi, Y., Saitoh, T., Yamagishi, A., and Yazawa, M. (2005). Critical regions for assembly of vertebrate nonmuscle myosin II. Biochemistry *44*, 174–183.

Rosenberg, M., and Ravid, S. (2006). Protein kinase C{gamma} regulates myosin IIB phosphorylation, cellular localization, and filament assembly. Mol. Biol. Cell *17*, 1364–1374.

Rosenberg, M., Straussman, R., Ben-Ya'acov, A., Ronen, D., and Ravid, S. (2008). MHC-IIB filament assembly and cellular localization are governed by the rod net charge. PLoS ONE *3*, e1496.

Saitoh, T., Takemura, S., Ueda, K., Hosoya, H., Nagayama, M., Haga, H., Kawabata, K., Yamagishi, A., and Takahashi, M. (2001). Differential localization of non-muscle myosin II isoforms and phosphorylated regulatory light chains in human MRC-5 fibroblasts. FEBS Lett. *509*, 365.

Sandquist, J. C., Swenson, K. I., Demali, K. A., Burridge, K., and Means, A. R. (2006). Rho kinase differentially regulates phosphorylation of nonmuscle myosin II isoforms A and B during cell rounding and migration. J. Biol. Chem. *281*, 35873–35883.

Sato, M. K., Takahashi, M., and Yazawa, M. (2007). Two regions of the tail are necessary for the isoform-specific functions of nonmuscle myosin IIB. Mol. Biol. Cell *18*, 1009–1017.

Simons, M., Wang, M., McBride, O. W., Kawamoto, S., Yamakawa, K., Gdula, D., Adelstein, R. S., and Weir, L. (1991). Human nonmuscle myosin heavy chains are encoded by two genes located on different chromosomes. Circ. Res. *69*, 530–539.

Straight, A. F., Cheung, A., Limouze, J., Chen, I., Westwood, N. J., Sellers, J. R., and Mitchison, T. J. (2003). Dissecting temporal and spatial control of cytokinesis with a myosin II inhibitor. Science *299*, 1743–1747.

Straussman, R., Even, L., and Ravid, S. (2001). Myosin II heavy chain isoforms are phosphorylated in an EGF-dependent manner: involvement of protein kinase C. J. Cell Sci. *114*, 3047–3057.

Tan, J. L., Ravid, S., and Spudich, J. A. (1992). Control of nonmuscle myosins by phosphorylation. Annu. Rev. Biochem. *61*, 721–759.

Trybus, K. M. (1991). Assembly of cytoplasmic and smooth muscle myosins. Curr. Opin. Cell Biol. *3*, 105–111.

Vicente-Manzanares, M., Zareno, J., Whitmore, L., Choi, C. K., and Horwitz, A. F. (2007). Regulation of protrusion, adhesion dynamics, and polarity by myosins IIA and IIB in migrating cells. J. Cell Biol. *176*, 573–580.

Wang, F., Kovacs, M., Hu, A., Limouze, J., Harvey, E. V., and Sellers, J. R. (2003). Kinetic mechanism of non-muscle myosin IIB: functional adaptations for tension generation and maintenance. J. Biol. Chem. *278*, 27439–27448.

Warrick, H. M., and Spudich, J. A. (1987). Myosin structure and function in cell motility. Annu. Rev. Cell Biol. *3*, 379–421.

Wei, Q., and Adelstein, R. S. (2000). Conditional expression of a truncated fragment of nonmuscle myosin II-A alters cell shape but not cytokinesis in HeLa cells. Mol. Biol. Cell *11*, 3617–3627.

Worthylake, R. A., and Burridge, K. (2003). RhoA and ROCK promote migration by limiting membrane protrusions. J. Biol. Chem. *278*, 13578–13584.